Ultrafast Time-Resolved Spectroscopy of Xanthophylls at Low Temperature

Hong Cong,[‡] Dariusz M. Niedzwiedzki,[†] George N. Gibson,[‡] and Harry A. Frank*[,†]

Department of Chemistry, University of Connecticut, U-3060, 55 North Eagleville Road, Storrs, Connecticut 06269-3060, and Department of Physics, University of Connecticut, U-3046, 2152 Hillside Road, Storrs, Connecticut 06269-3046

Received: August 8, 2007; In Final Form: January 7, 2008

Many of the spectroscopic features and photophysical properties of xanthophylls and their role in energy transfer to chlorophyll can be accounted for on the basis of a three-state model. The characteristically strong visible absorption of xanthophylls is associated with a transition from the ground state S_0 ($1^1A_g^-$) to the S_2 ($1^1B_u^+$) excited state. The lowest lying singlet state denoted S_1 ($2^1A_g^-$), is a state into which absorption from the ground state is symmetry forbidden. Ultrafast optical spectroscopic studies and quantum computations have suggested the presence of additional excited singlet states in the vicinity of S_1 ($2^1A_g^-$) and S_2 ($1^1B_u^+$). One of these is denoted S* and has been suggested in previous work to be associated with a twisted molecular conformation of the molecule in the S_1 ($2^1A_g^-$) state. In this work, we present the results of a spectroscopic investigation of three major xanthophylls from higher plants: violaxanthin, lutein, and zeaxanthin. These molecules have systematically increasing extents of π-electron conjugation from nine to eleven conjugated carbon−carbon double bonds. All-trans isomers of the molecules were purified by high-performance liquid chromatography (HPLC) and studied by steady-state and ultrafast time-resolved optical spectroscopy at 77 K. Analysis of the data using global fitting techniques has revealed the inherent spectral properties and ultrafast dynamics of the excited singlet states of each of the molecules. Five different global fitting models were tested, and it was found that the data are best explained using a kinetic model whereby photoexcitation results in the promotion of the molecule into the S_2 ($1^1B_u^+$) state that subsequently undergoes decay to a vibrationally hot S_1 ($1^1A_g^-$) state and with the exception of violaxanthin also to the S* state. The vibrationally hot S_1 ($1^1A_g^-$) state then cools to a vibrationally relaxed S_1 ($2^1A_g^-$) state in less than a picosecond. It was also found that a portion of the S* population is converted into S_1 ($2^1A_g^-$) during deactivation, but this process and the relative yield of S* was found to depend on temperature, consistent with it being associated with a twisted conformation of the xanthophyll. The results of the global fitting suggest that subpopulations of twisted conformers of xanthophylls already exist in the ground state prior to photoexcitation.

Introduction

Xanthophylls are oxygenated carotenoids that play an important role in photosynthesis as light-harvesting pigments.[1] They are strong absorbers of solar energy in the 450−550 nm region of the visible spectrum where chlorophyll (Chl) is not a very efficient absorber.[2] Xanthophylls also stabilize protein structures, regulate energy flow among different pigment−protein complexes, and dissipate potentially deleterious excess energy absorbed by the photosynthetic apparatus.[3−5] Understanding the mechanism by which xanthophylls deactivate excited-state energy requires a thorough knowledge of the energetics and photophysics of their excited electronic states. Because the excited states of these molecules decay with time constants in the range of 100 fs to 10 ps, ultrafast laser spectroscopic techniques are required to monitor the photoprocesses. Many excellent spectroscopic investigations involving highly innovative and sophisticated approaches have been reported in the literature on xanthophylls and carotenes,[6−11] but the ordering and nature of the excited states and the pathways of deactivation remain contentious.[10]

It is generally agreed that the energy level ordering of xanthophylls is similar to model polyenes and carotenoids.[12−15] (See Figure 1.) The lowest-lying excited singlet state, S_1, is described by the group theoretical representation, $2^1A_g^-$, where the minus sign indicates the pseudoparity character of the state.[16−18] The ground state, S_0, has the same symmetry as S_1 and is denoted $1^1A_g^-$. One-photon transitions between S_0 ($1^1A_g^-$) and S_1 ($2^1A_g^-$) are forbidden according to both group theoretical ($g \leftrightarrow u$) and pseudoparity ($+ \leftrightarrow -$) selection rules.[18] The transition responsible for the strong visible absorption of xanthophylls is an S_0 ($1^1A_g^-$) → $1^1B_u^+$ transition. The $1^1B_u^+$ state is often referred to as S_2, but theoretical[19,20] and experimental[6−9,11,21−31] reports suggest other excited states may lie near or between S_1 ($2^1A_g^-$) and S_2 ($1^1B_u^+$). (See Polivka and Sundstrom[10] for a recent review of this topic.) Because the nature and positions of these additional states are still unclear and also depend on the carotenoid, we shall use the traditional notation S_0 ($1^1A_g^-$), S_1 ($2^1A_g^-$), and S_2 ($1^1B_u^+$) to describe the fundamental energy level scheme (Figure 1).

The present work addresses the mechanism of excited-state deactivation of xanthophylls with particular attention to the properties and identity of S*. S* is a state designation introduced by van Grondelle and co-workers[6] to account for the observation that the carotenoid, spirilloxanthin, in solution and in the LH1 complex from *Rhodospirillum rubrum*, showed different decay

* Author to whom correspondence should be addressed. Fax: 860-486-6558. E-mail: harry.frank@uconn.edu.
† Department of Chemistry.
‡ Department of Physics.

10.1021/jp0763681 CCC: $40.75
Published on Web 02/23/2008

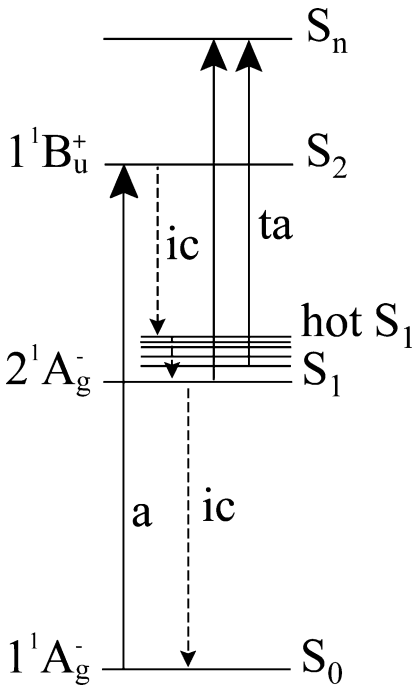

Figure 1. Energy level scheme of the xanthophylls and associated photophysical processes: a, absorption; ta, transient absorption; ic, internal conversion.

time constants and distinct spectral features as a function of probe wavelength. The model proposed by these authors was that after photoexcitation, S_2 ($1^1B_u^+$) undergoes a branched decay in ~200 fs to both S_1 ($2^1A_g^-$) and S*. Thus, S* was postulated to be an excited-state that provides an alternate path for the depopulation of S_2 ($1^1B_u^+$). In addition, in LH1 and LH2 pigment−protein complexes, S* was reported to lead to triplet state formation via ultrafast singlet−triplet homofission.[6−8,10,11,15,29,30,32,33] The spectral profile of S* consists of a broad featureless transient absorption band appearing on the long wavelength side of the steady-state S_0 ($1^1A_g^-$) → S_2 ($1^1B_u^+$) absorption spectrum. Alternatively, it has been described as a "blue shoulder" on the short wavelength side of the strong S_1 ($2^1A_g^-$) → S_n transient absorption band.[6,7,10,29,30,34] In addition to populating S*, deactivation from the S_2 ($1^1B_u^+$) state also populates a vibrationally hot S_1 ($2^1A_g^-$) state (Figure 1), whose S_1 ($2^1A_g^-$) → S_n excited-state transient absorption profile is broader and its peak position red-shifted in comparison with that of the relaxed S_1 ($2^1A_g^-$) state. The vibrationally hot S_1 ($2^1A_g^-$) relaxes within several hundreds of femtoseconds.[31,35−37] For most xanthophylls, S* and S_1 ($2^1A_g^-$) decay to the ground state in the range of 1−40 ps.[11]

In the present work, ultrafast time-resolved spectroscopy was carried out at 77 K to examine the spectroscopic properties and dynamics of three major xanthophylls from green plants, violaxanthin, lutein, and zeaxanthin (Figure 2). These molecules have nine, ten and eleven conjugated carbon−carbon double bonds, *N*, respectively. Previous room-temperature ultrafast spectroscopic investigations performed in our laboratory[11] on these and other xanthophylls in conjunction with quantum mechanical computations have supported the model of Van Grondelle and co-workers[6−8,33] that S* is simply an excited-state of the molecule formed via a branched pathway from higher excited singlet states. In addition, we have proposed that S* is an S_1 ($2^1A_g^-$) state having a twisted conformational geometry relative to the ground state.[11] A critical test of this model is provided in the present study that examines the spectra and dynamics of S* and S_1 ($2^1A_g^-$) at low temperature where it is expected that the effect of conformational twisting should be altered by freezing and manifested in these experimental observables.

Materials and Methods

Sample Preparation. Violaxanthin, lutein, and zeaxanthin were isolated and purified as described previously.[11]

Spectroscopy at Cryogenic Temperatures. The molecules were dissolved in EPA (5/5/2, v/v/v, diethyl ether/isopentane/ethanol) to an OD of 0.3 at the maximum of their steady state absorption in a 2 mm path cuvette. Transient absorption spectra and temporal profiles were measured using a femtosecond spectrometer system described in detail previously.[31,38] A helium cryostat (Janis Model STVP100) was used to achieve the low sample temperature. The xanthophylls were excited using a pump beam obtained from an optical parametric amplifier (Spectra-Physics) with a pulse duration of ~100 fs, and the probe laser pulses were derived from a white light continuum generated by a nonlinear crystal (Ultrafast Systems LLC). The energy of the excitation pulses was 1 μJ/pulse delivered at 1 kHz and directed into the lowest energy vibronic band (0−0) associated with the absorption spectra in the EPA glasses at 77 K. The spot size of the pump pulse was 1.2 mm in diameter, and the intensity was ~2.2×10^{14} photons·cm^{-2}·$pulse^{-1}$. The excitation wavelengths were 484 nm for violaxanthin, 491 nm for lutein, and 500 nm for zeaxanthin. Surface Explorer software (v.1.0.4) was used to correct the dispersion of the transient absorption spectra. ASUFit 3.0 software provided by Dr. Evaldas Katilius at Arizona State University was modified for specific types of global fitting and target analysis as described below. The quality of the fitting was evaluated using the residual parameter chi square, χ^2.

Results

The steady state absorption spectra of violaxanthin ($N = 9$), lutein ($N = 10$), and zeaxanthin ($N = 11$) (Figure 2) taken in pyridine at room temperature[11] and at 77 K in an EPA glass are shown in Figure 3. At 77 K, the spectra display a much higher degree of vibronic resolution than seen at room temperature. For all the molecules, multiple vibronic bands are observed, and the Franck−Condon maximum shifts from the (0−1) band at room temperature to the (0−0) vibronic feature as the temperature is lowered. Also, the spectra of the molecules shift to longer wavelength and the vibronic resolution decreases with increasing *N*.

Transient absorption spectra of the xanthophylls taken in an EPA glass at 77 K at four delay times, 100 fs, 500 fs, 2 ps, and 10 ps after the excitation pulse are shown in Figure 4. The signals are considerably sharper at 77 K compared to those taken at room temperature.[11] The negative signals in the region 470 to 520 nm correspond to a bleaching of the strongly allowed S_0 ($1^1A_g^-$) → S_2 ($1^1B_u^+$) absorption band that persists to some degree until the molecules ultimately return back to the ground state in times longer than 10 ps. The pronounced transient absorption signal in the region 520 to 600 nm is associated with an S_1 ($2^1A_g^-$) → S_n transition, which shifts to longer wavelength as *N* increases. A closer look at the spectra taken at the 500 fs time delay reveals broadening on the long-wavelength side of the major peak that disappears as time elapses beyond 2 ps (Figure 4).

Global Analysis. The datasets obtained from the transient absorption experiments are a collection of measurements taken at different wavelengths, λ, and different times, *t*, after excitation.

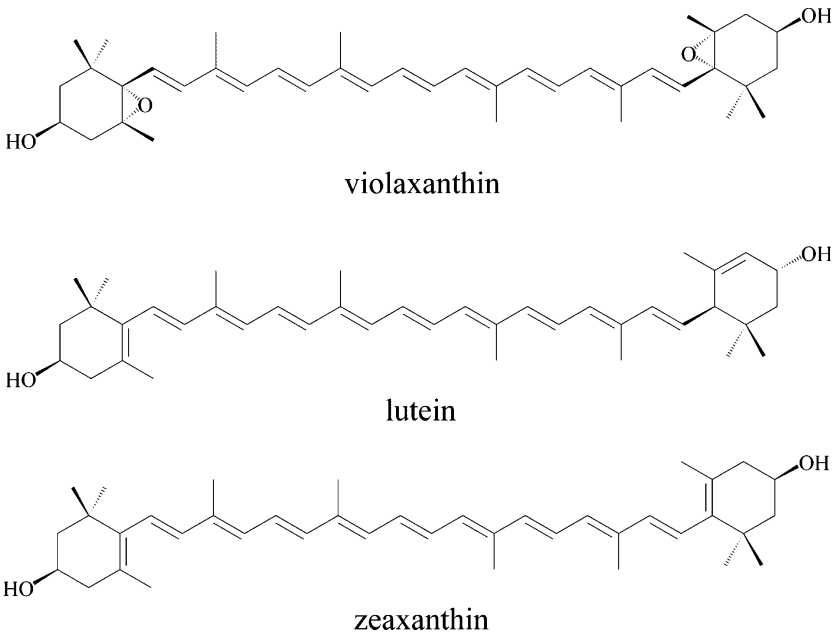

Figure 2. Structures of all-trans isomers of violaxanthin, lutein, and zeaxanthin.

This set of time-resolved spectra, denoted $\Psi(t, \lambda)$, is a superposition of the contributions of n different components

$$\Psi(t, \lambda) = \sum_{l=1}^{n} c_l(t)\epsilon_l(\lambda) \quad (1)$$

where $c_l(t)$ and $\epsilon_l(\lambda)$ denote the concentration and spectrum, respectively, of component l, representing one state of the molecule.[39] After correcting for dispersion in the raw spectral data, the number of principle components can be found via singular value decomposition.

Because the quantity that will be computed in the global fitting analysis is the product $c_l(t)\epsilon_l(\lambda)$, the method does not determine $c_l(t)$ and $\epsilon_l(\lambda)$ independently. However, as shown by van Stokkum et al.[39] the shape of $c_l(t)$ can be correlated with a certain kinetic model in the form

$$\frac{\mathrm{d}}{\mathrm{d}t} c(t) = Kc(t) + j(t) \quad (2)$$

where K is the matrix of rate constants for deactivation of different excited states of the molecule, and $j(t)$ is the input vector to the system. The details of the solution to this equation are given in the Supporting Information.

To understand the mechanism of excited-state decay of the xanthophylls, various kinetic models (Figure 5) may be tested using this global fitting formalism. On the basis of previous work, four excited states are included: S_2 ($1^1B_u^+$), vibrationally hot S_1 ($2^1A_g^-$) (denoted S_1'), S*, and vibrationally relaxed S_1 ($2^1A_g^-$).

Parallel Model. Initially, a model assuming parallel noninteracting pathways (Figure 5A) was applied to obtain the order of the kinetics, that is, the number of independent parameters that need to be fitted simultaneously to simulate the experimental data. This model also yields the lifetimes of the different excited states. Minimization of the χ^2 parameter was applied to optimize the fitting. The residual plots of the kinetics and spectral traces comparing the fit and experimental data were then viewed to determine whether the order of the kinetics was sufficient and whether the fitting was acceptable. In this case the fitted data are referred to as decay-associated difference spectra (DADS), the results of which for the xanthophylls are given in Figure 6. It is important to note that because the spectra of the kinetic components presented in Figure 6 are not weighted by their associated extinction coefficients, which are not available, the DADS presented here are simply amplitude profiles of preexponential factors.

For all three molecules, the initial DADS corresponds to the spectral change associated with the molecule entering the excited S_2 ($1^1B_u^+$) state. This first DADS is characterized by a negative, ground-state bleaching between 470 and 520 nm, and it is accompanied by several other negative peaks between 520 and 650 nm due primarily to stimulated emission from S_2 ($1^1B_u^+$). A second DADS in all cases has a complex line shape including a negative band at shorter wavelengths, a zero crossing, and positive amplitude at longer wavelengths. The final DADS shows the familiar, strongly allowed, vibronically relaxed, positive amplitude spectrum associated with the S_1 ($2^1A_g^-$) $\rightarrow$ S_n transition of the carotenoids. For violaxanthin, only three kinetic components were necessary to achieve a good fit to the data. For lutein and zeaxanthin, however, an additional DADS component was necessary. This component exhibited a lifetime of 10.2 ps for lutein and 8.2 ps for zeaxanthin at 77 K and showed a wavy line shape with at least two positive and two negative bands.

If the decay from S_2 ($1^1B_u^+$) takes place via a branched pathway,[6] the parallel model is an oversimplification, and the DADS components will not represent real, physical, spectroscopic profiles of the transient species. There are many alternatives to the parallel model, and all of them will have nondiagonal K matrices. The explicit mathematical forms of these alternate matrices are given in the Supporting Information.

Sequential Model. Among the models having nondiagonal K matrices, the simplest is the sequential model (Figure 5B). In this case, the molecules decay from one excited-state to another in a nonbranching, unidirectional, irreversible way. The results of fitting to this model are referred to as evolution-associated difference spectra (EADS) and are shown in Figure 7.

As noted above for violaxanthin, only three kinetic components were needed to yield an excellent fit to the data. However, for lutein and zeaxanthin four components were required for an acceptable fit. For all three xanthophylls, the initial EADS

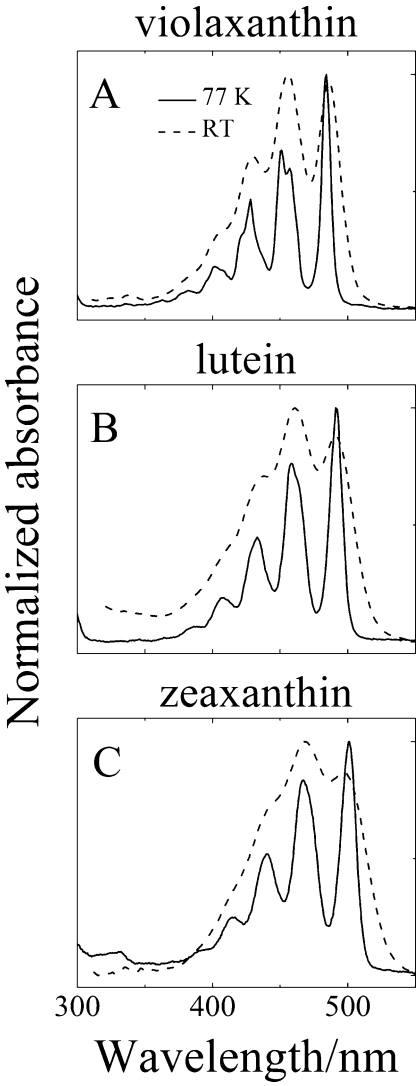

Figure 3. Steady-state absorption spectra of (A) violaxanthin, (B) lutein, and (C) zeaxanthin in pyridine at room temperature[11] and in EPA at 77 K.

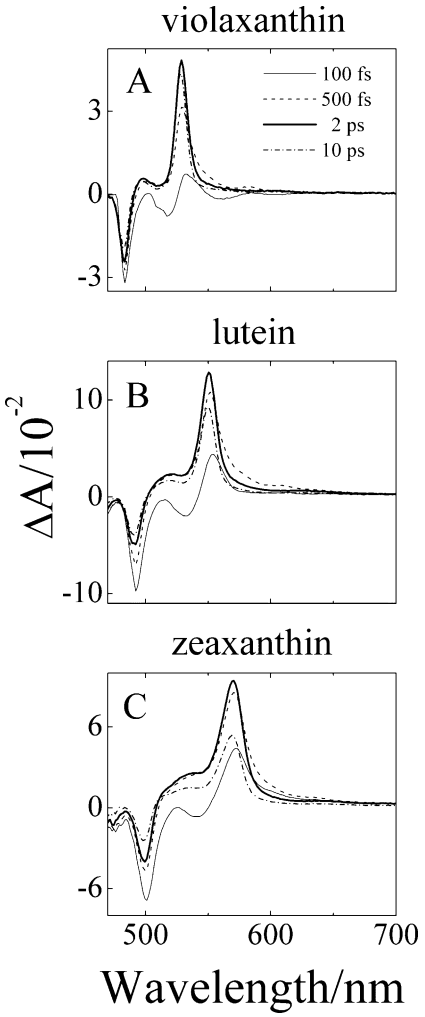

Figure 4. Transient absorption spectra of the xanthophylls taken in EPA at 77 K at different time delays after excitation into the (0−0) vibrational level of the S_2 state.

is characterized by a negative band between 470 and 520 nm indicating bleaching of the S_0 ($1^1A_g^-$) → S_2 ($1^1B_u^+$) transition. Also, several other negative peaks occur between 520 and 650 nm. These are due to stimulated emission from S_2 ($1^1B_u^+$). The second EADS component displays a very broad, positive line shape (dashed lines in Figure 7) between 525 and 625 nm that extends to significantly longer wavelength. The second EADS corresponds to a kinetic component whose decay becomes faster with increasing *N*, that is, 1.4 ps to 560 fs to 460 fs at 77 K (Figure 7). The final EADS component shows features associated with the strongly allowed, vibronically relaxed, positive amplitude S_1 ($2^1A_g^-$) → S_n spectrum. Thus, the time constant for this component corresponds to the lifetime of the S_1 ($2^1A_g^-$) state. The values are observed to be about 5 ps longer at 77 K than at room temperature.[34,36,40−43 11] (See Table 1.) As alluded above for lutein and zeaxanthin, an additional EADS component with a time constant between the second and fourth EADS was needed for an acceptable fit to the data (dark solid lines in Figure 7B,C). This component shows a very strong positive band between 550 and 575 nm. The time constant of this component decreases from 10.2 to 8.2 ps at 77 K in going from lutein to zeaxanthin. Also, in going from the third to the fourth EADS, the ground state bleaching below 500 nm partially recovers indicating that a portion of the population has relaxed from an excited state to the ground state.

Target Models. Previous work has shown convincingly that both S_1 ($2^1A_g^-$) and S* are formed from a branched decay pathway originating from S_2 ($1^1B_u^+$).[6,10,11,44] Therefore, neither a purely parallel (DADS) nor a purely sequential (EADS) model is entirely correct for describing the photophysics of excited-state deactivation. To determine the underlying mechanism of excited-state decay, target analysis is required that allows examining mechanisms that utilize a combination of parallel and sequential pathways. Three different target models have been explored here that also examine the possibility of transfer to and from the S* and S_1 ($2^1A_g^-$) states. The explicit mathematical forms of the *K* matrices for these models are presented in the Supporting Information. The results of fitting to a target model are referred to as species-associated difference spectra (SADS).

The target analysis described here will be restricted to lutein and zeaxanthin only. Violaxanthin is not included because only three kinetic components were needed to obtain excellent fits to the spectral and temporal data for this molecule. Neither the dynamics nor the lineshapes observed for violaxanthin indicate any evidence for the formation of S* at 77 K consistent with the report of its very low yield at room temperature.[11] Thus, a completely adequate and appropriate "target" model for explaining the excited-state decay mechanism of violaxanthin is the

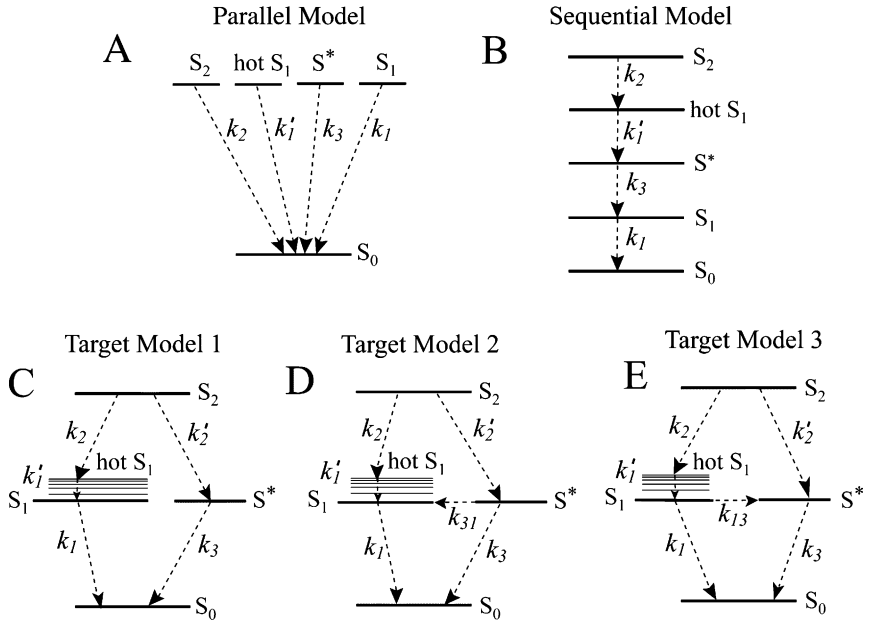

Figure 5. Global fitting models tested using the ultrafast transient absorption spectral datasets.

sequential (EADS) model based on the pathway S_2 ($1^1B_u^+$) → hot S_1 ($2^1A_g^-$) → relaxed S_1 ($2^1A_g^-$) → S_0 ($1^1A_g^-$). For lutein and zeaxanthin, where four kinetic components are required for good fits to the datasets and where spectroscopic features associated with the formation of S* are observed both at room[11] and low temperatures, this is not the case, and a more elaborate target model is needed.

Target Model 1. As stated above Van Grondelle et al.[6] originally proposed that for spirilloxanthin ($N = 13$) S* is formed via a branched decay pathway from S_2 ($1^1B_u^+$) independent and noninteracting with an alternate branch, whereby S_2 ($1^1B_u^+$) decays to S_1 ($2^1A_g^-$). More recent findings indicate that S_2 ($1^1B_u^+$) decays to a vibrationally hot S_1 ($2^1A_g^-$) state followed by vibrational cooling in S_1 ($2^1A_g^-$).[31,35−37] In this case, there will be five rate constants and four excited states (Figure 5C). In the analysis using this model, the total decay rate constant from S_2 ($1^1B_u^+$), ($k_2 + k_2'$), was allowed to vary while k_2' was changed manually to obtain the best fit based on the χ^2 parameter and the resultant shapes of the target amplitude components. The analysis revealed that the values of k_2 and k_2' were very similar. However, a major problem with this model was that the fitted profile had negative peaks in the wavelength region where the S_1 ($2^1A_g^-$) → S_n transition shows strong absorption. Because the S* → S_n and S_1 ($2^1A_g^-$) → S_n absorption bands should be entirely positive, this target model was deemed unacceptable. Taking a clue from the fact that the sequential (EADS) model (Figure 5B and 7), which naturally includes population transfer from S* to S_1 ($2^1A_g^-$) and shows the third kinetic component to be entirely positive, a second target model invoking S* → S_1 ($2^1A_g^-$) transfer was tested.

Target Model 2. In this model, population transfer from S* to S_1 ($2^1A_g^-$) with decay rate constant k_{31} was added to target model 1 as shown in Figure 5D. Figure 8 gives the fitting results according to this model. The outcome is much more reasonable than target model 1. The absorption transitions all exhibit positive bands and those associated with S* and S_1 ($2^1A_g^-$) are clearly distinguished by the third (dark solid lines in Figure 8) and fourth (thin solid lines in Figure 8) SADS components, respectively. A very slight dip in the region near the maximum of the S* → S_n transition is seen in the second SADS for zeaxanthin (dashed line in Figure 8D), which is the line shape

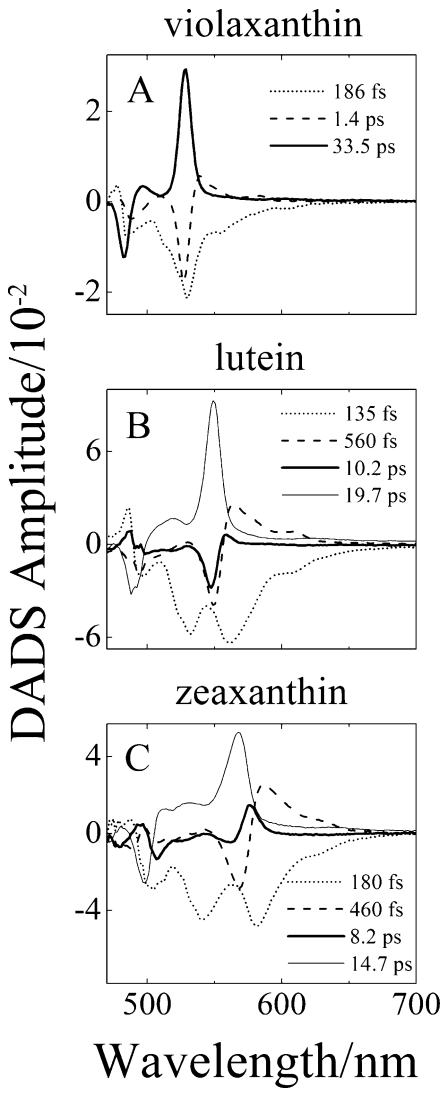

Figure 6. Decay-associated difference spectra (DADS) obtained from the transient absorption datasets represented in Figure 4 using the parallel model of global fitting (Figure 5 panel A).

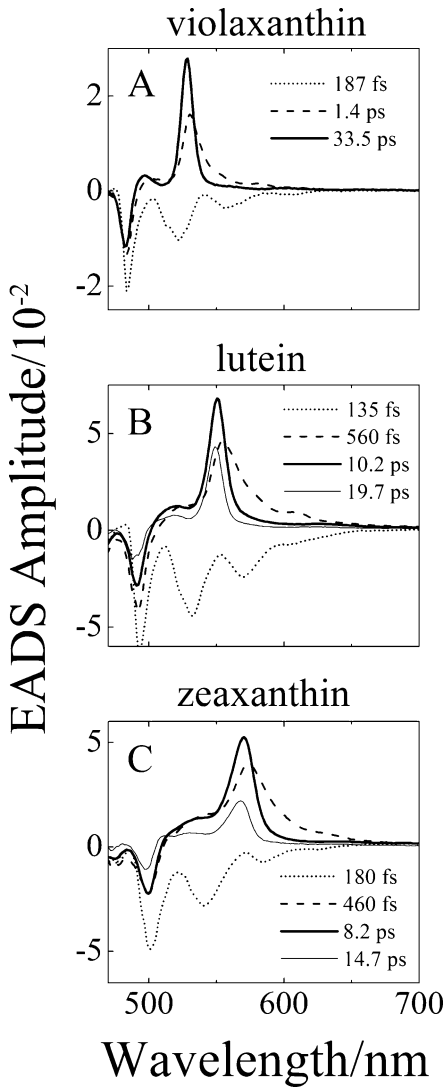

Figure 7. Evolution-associated difference spectra (EADS) obtained from the transient absorption datasets represented in Figure 4 using the sequential model of global fitting (Figure 5, panel B).

associated with the transition from vibrationally hot S_1 ($2^1A_g^-$) to S_n. This small interference is expected because hot S_1 ($2^1A_g^-$) and S* compete for population from S_2 ($1^1B_u^+$). The feature was minimized when the rate constants, k_2 and k_2', affecting the branching ratio of S* to hot S_1 ($2^1A_g^-$) formation were very similar.

Target Model 3. Because S_1 ($2^1A_g^-$) and S* may be very close in energy, suggested by the fact that in some cases they have rather similar lifetimes (e.g., for zeaxanthin at 77 K the values derived from target model 2 (Figure 8D) are 8.2 ps for S* and 14.7 ps for S_1 ($2^1A_g^-$)), it raises the question of whether there could be population transfer from S_1 ($2^1A_g^-$) to S*. Thus, a third model enabling branching from S_1 ($2^1A_g^-$) to S* and assigned a decay rate constant k_{13} (Figure 5E) was tested. Similar to the previous target models, the total decay rate constant for S_1 ($2^1A_g^-$), ($k_{13} + k_1$), was allowed to vary while decay rate constant k_1 from S_1 ($2^1A_g^-$) to S_0 ($1^1A_g^-$) was adjusted manually to obtain the best fit. When this model was applied to the 77 K datasets, it was found that when k_{13} was set to zero, the solution was precisely the same as target model 1, as expected. As k_{13} was increased, S_1 ($2^1A_g^-$) population was preferentially transferred to S* instead of repopulating S_0 ($1^1A_g^-$). However, the amplitude of the fourth SADS associated with the S_1 ($2^1A_g^-$) $\rightarrow$ S_n transition became negative (data not shown). Because the line shape of the S_1 ($2^1A_g^-$) $\rightarrow$ S_n transition must be entirely positive, target model 3 invoking population transfer from S_1 ($2^1A_g^-$) $\rightarrow$ S* was ruled out.

The global fitting models tested here all include the path of excited-state deactivation from S_2 ($1^1B_u^+$) to a vibrationally hot S_1 ($2^1A_g^-$) state. One might argue then that there should also be decay from S_2 ($1^1B_u^+$) to a vibrationally hot S* state. A model including this pathway was tested, but the results were deemed unreasonable due to the fit converging on a solution that included an unreasonably long (>50 ps) lifetime component having a very small amplitude despite the fact that the initial parameter for decay from the vibrationally hot S* to the relaxed S* state was set in the expected range of hundreds of femtoseconds.

Discussion

It is expected on the basis of simple quantum mechanical models of π-electron conjugated systems that the absorption spectra of carotenoids will shift to longer wavelength as the conjugation length of the molecule increases.[15,45,46] This is indeed the case in going from violaxanthin ($N = 9$) to lutein ($N = 10$) to zeaxanthin ($N = 11$) (Figure 3). The reduction in vibronic resolution with increasing N may be attributed to an increase in conformational disorder brought about by the presence of terminal β-rings in conjugation with the extended polyene chain.[47,48] The presence of the epoxide groups in violaxanthin effectively removes the rings from the conjugated system, and thus this molecule shows the highest degree of spectral resolution (narrowest bands). The one β-ring in lutein and the two β-rings in zeaxanthin widen the distribution of conformations along the π-electron conjugated chain, which along with disorder arising from environmental variations in the solvent also lead to broadening of the spectral profile. Lowering the temperature of the xanthophylls to 77 K results in narrowing of the spectral lines owing to the fact that the populations of the S_0 ($1^1A_g^-$) and S_2 ($1^1B_u^+$) states are effectively condensed to the lower vibronic levels. This also explains why the Franck−Condon maxima in the steady-state spectra shown in Figure 3 shift from the (0−1) band at room temperature to the (0−0) band at 77 K.[49−51]

Analogous to the steady-state spectra shown in Figure 3 and for the same reasons discussed above, the main positive absorption band in the transient lineshapes shown in Figure 4 red-shifts and broadens with increasing N, but narrows upon cooling the samples from room temperature to 77 K. Transient absorption spectra taken at a 500 fs delay time both at room temperature[11] and at 77 K (Figure 4) show broadening of the main band that is absent from the spectra taken at 2 ps. All of the global fitting models tested here (Figures 6−8) reveal this broadening to be associated with a distinct kinetic component having a major positive band slightly red-shifted from the strong S_1 ($2^1A_g^-$) $\rightarrow$ S_n transient absorption band appearing at longer times. The values for the time constant of the broad band range from 460 fs to 1.4 ps. The origin of this component is revealed by the position of small bands observed ~50 nm to longer wavelength of the major feature, clearly seen in the second DADS, EADS, and SADS (dashed lines in Figures 6−8) of the xanthophylls. For all the xanthophylls, the energy separation between this small peak and the major positive feature falls within a narrow range of 1700 ± 30 cm^{-1} (violaxanthin, 1670 cm^{-1}; lutein, 1684 cm^{-1}; and zeaxanthin, 1720 cm^{-1}). Absorption spectra of carotenoids are dominated by vibronic bands associated with symmetric carbon−carbon single bond (−C−C−) and double bond (−C═C−) stretches having constant

TABLE 1: Lifetimes of the S_1 (τ_1), Vibrationally Hot S_1 (τ_1'), S_2 (τ_2), and S* (τ_3) States of Violaxanthin, Lutein, and Zeaxanthin

molecule	pump λ (nm)	probe λ (nm)	τ_1 (ps)	τ_1' (fs)	τ_2 (fs)	τ_3 (ps)	τ_s[a] (fs)	fitting method	solvent	T/K	reference
violaxanthin	484	cont[b]	33.5 ± 0.1	1.4 ± 0.1	187 ± 5	n.a.[c]	120	global fit	EPA	77 K	this work
	485	cont	26.4 ± 0.1	685 ± 5	173 ± 5	n.a.	138	global fit	pyridine	RT[d]	this work
	485	cont	26.1 ± 0.1	582 ± 6	163 ± 1	5.0 ± 0.2	128	global fit	pyridine	RT	11
	485	543	25.5 ± 0.2	n.a.	n.a.	2.0 ± 0.6	n.a.	single λ	pyridine	RT	11
	420	512	23.9	n.d.[f]	n.d.	n.e.	300	single λ	n-hexane	RT	40
	480	var[e]	24.6 or 25.3	320−380	n.d.	n.e.	200	single λ	methanol	RT	41
lutein	491	cont	19.7 ± 0.1	560 ± 7	135 ± 5	10.2 ± 0.2	130	global fit	EPA	77	this work
	491	cont	15.6 ± 0.1	414 ± 6	135 ± 5	2.9 ± 0.1	125	global fit	pyridine	RT	this work
	491	cont	15.6 ± 0.1	435 ± 5	127 ± 3	2.9 ± 0.1	121	global fit	pyridine	RT	11
	491	571	15.8 ± 0.1	n.a.	n.a.	2.2 ± 0.4	n.a.	single λ	pyridine	RT	11
	490	528	15	n.d.	n.d.	n.e.	∼150	single λ	methanol	RT	42
zeaxanthin	500	cont	14.7 ± 0.1	460 ± 10	180 ± 5	8.2 ± 0.2	110	global fit	EPA	77	this work
	497	cont	10.1 ± 0.1	322 ± 6	145 ± 5	2.9 ± 0.1	175	global fit	pyridine	RT	this work
	497	cont	10.2 ± 0.2	370 ± 5	146 ± 2	2.8 ± 0.2	130	global fit	pyridine	RT	11
	497	596	10.3 ± 0.1	n.a.	n.a.	n.e.[g]	n.a.	single λ	pyridine	RT	11
	266	cont	9.8 ± 1.0	700 ± 70	180 ± 36	4.9 ± 0.5	120−160	global fit	methanol	RT	34
	400	cont	9.0 ± 0.9	350 ± 40	70 ± 14	2.8 ± 0.3	120−160	global fit	methanol	RT	34
	485	cont	9.2 ± 0.9	350 ± 40	135 ± 27	n.e.	120−160	global fit	methanol	RT	34
	490	var	8.6 or 8.8	220 or 230	n.d.	n.e.	200	single λ	methanol	RT	41
	420	540	9.0	n.d.	n.d.	n.e.	300	single λ	n-hexane	RT	40
	490	555	9.0	n.d.	n.d.	n.e.	∼150	single λ	methanol	RT	42
	490	484	9.0	300	n.d.	n.e.	∼150	single λ	n-hexane	RT	36
	490	547	9.6	n.d.	270	n.e.	∼150	single λ	n-hexane	RT	36
	490	577	9.1	800	200	n.e.	∼150	single λ	n-hexane	RT	36
	490	481	9.0	200	n.d.	n.e.	∼150	single λ	methanol	RT	36
	490	548	9.1	n.d.	280	n.e.	∼150	single λ	methanol	RT	36
	490	579	9.0	540	120	n.e.	∼150	single λ	methanol	RT	36
	485	560	9.3	n.d.	290	n.e.	∼100	single λ	ethanol	RT	43

[a] τ_s is the instrument response time. [b] White light continuum. [c] Not applicable. [d] Room temperature. [e] Various. [f] Not determined. [g] Not evident.

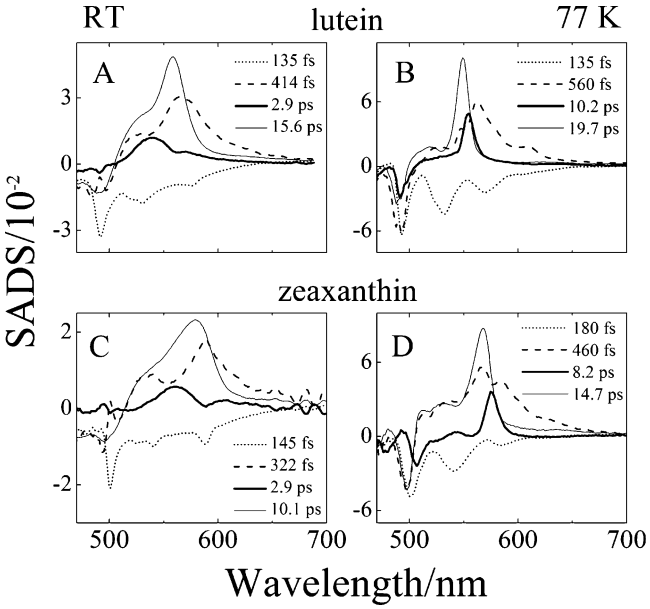

Figure 8. Global fitting results obtained from the transient absorption datasets for lutein and zeaxanthin in pyridine at RT[11] and in EPA at 77 K (Figure 4) using target model 2 (Figure 5, panel D).

frequencies of ∼1200 and ∼1600 cm^{-1}, respectively. However, resonance Raman and fluorescence spectroscopy carried out on all-trans-β-carotene[36,52,53] and longer polyenes[54,55] have revealed −C═C− stretching frequencies 100−200 cm^{-1} higher than this for molecules in the S_1 ($2^1A_g^-$) state. Thus, as previously discussed in detail for open-chain carotenoids[31] the frequency and constant energy separation of the small band relative to the major peak are consistent with an assignment of the small peak to a (low-energy) transition from an upper vibronic level of S_1 ($2^1A_g^-$) to a higher singlet state, S_n (see Figure 1). This observation, taken together with the fact that the entire line shape of this rapidly decaying kinetic component is very broad, strongly supports the idea that it is associated with a vibrationally hot S_1 ($2^1A_g^-$) → S_n transition. Such a transition is expected to be broader and red-shifted compared to transitions originating from a vibrationally relaxed S_1 ($2^1A_g^-$) state.[11,35−37]

Of the models tested here, target model 2 (Figure 5D) works best to account for the data from lutein and zeaxanthin. The global fits are shown in Figure 8 and the S_1 ($2^1A_g^-$) and S* state lifetimes obtained from this model are summarized in Figure 9. The initial SADS (dotted lines in Figure 8) are a combination of bleaching of S_0 ($1^1A_g^-$) → S_2 ($1^1B_u^+$) transition and stimulated emission from S_2 ($1^1B_u^+$). As mentioned in the above paragraph, the second SADS (dashed lines in Figure 8) show a broad line shape attributed to a vibronically hot S_1 ($2^1A_g^-$) → S_n transition.[11,35−37] The rate of decay of this component becomes faster with increasing N for the molecules at room temperature[11] and at 77 K is decreasing from 1.4 ps for violaxanthin (Table 1) to 560 fs for lutein to 460 fs for zeaxanthin (Table 1 and Figure 9). For a given molecule, the rate of decay is slower at 77 K compared to room temperature, which is consistent with vibrational cooling of a hot S_1 ($2^1A_g^-$) state to a relaxed state. The dependence on N is probably due to increased vibronic activity that promotes nonradiative dissipation more effectively as the π-electron chain length gets longer. The enhanced rate of decay with increasing N may also be facilitated by the presence of the terminal rings in conjugation, which as discussed above, contribute to conformational disorder that broadens the vibronic profiles of the steady state and transient spectra.

For lutein and zeaxanthin, the third SADS (dark solid lines in Figure 8) are representative of the S* → S_n transition, and in global fits of the room-temperature data (Figure 8A,C) the band maximum appears on the short wavelength side of the major S_1 ($2^1A_g^-$) → S_n transient absorption band. However, as the temperature is lowered to 77 K (Figure 8B,D) the feature

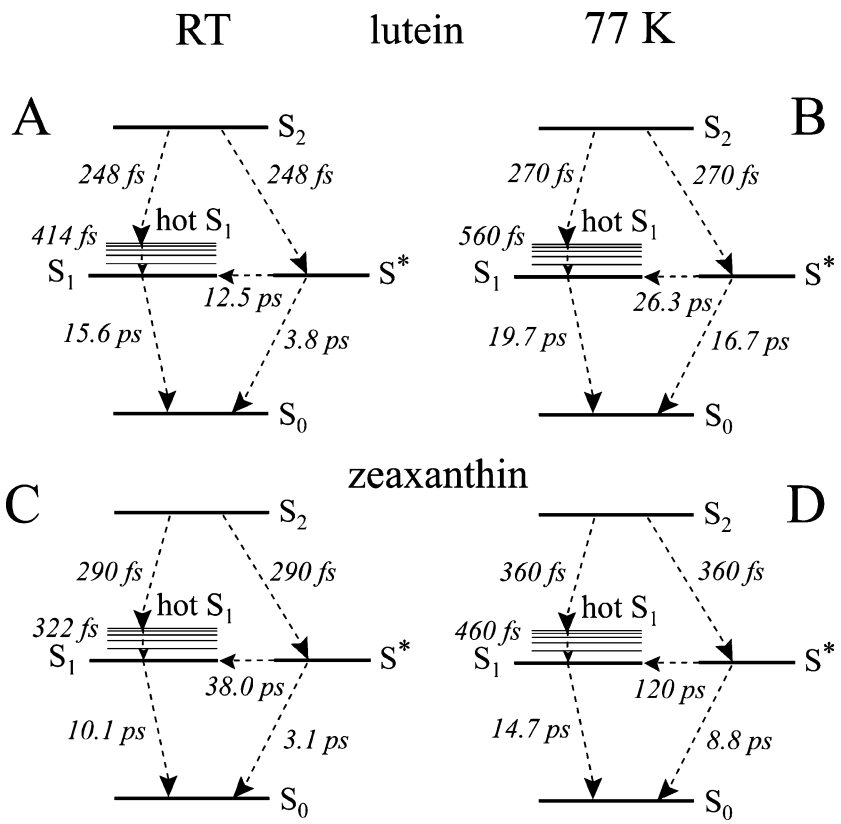

Figure 9. Summary of the excited-state lifetimes obtained from the kinetic rate constants used to fit target model 2 (Figure 5, panel D) to the transient absorption datasets for lutein and zeaxanthin.

associated with S* narrows, and its maximum moves to the long wavelength side of the major S_1 ($2^1A_g^-$) → S_n transient absorption band. This would be expected if the S* → S_n band profile at room temperature is broadened due to conformational disorder. As discussed above for the steady-state spectra and illustrated in Figure 3, lowering the temperature reduces conformational disorder, results in narrowing of the spectral lines, and accounts for why the maximum of the bands shifts to longer wavelength. The positions of the maxima in the third SADS are very likely representative of the spectral origins of the S* → S_n transitions. Also, this third SADS component has a time constant of 10.2 ps for lutein and 8.2 ps for zeaxanthin at 77 K, which are approximately three times longer than the values obtained from the room-temperature data (Table 1). This indicates that the vibronic modes promoting the decay are less populated at the low temperature.

The fourth SADS (thin solid line in Figure 8) reveals the lifetimes of the S_1 ($2^1A_g^-$) state for the molecules. These are observed to be slightly longer at 77 K than at room temperature. Once again, this is most likely due to the less efficient population of promoting modes of decay at the low temperature. The dependence of the S_1 ($2^1A_g^-$) state dynamics on N is also well known to follow the predictions based on the energy gap law for radiationless transitions.[56,57]

As discussed above, for lutein and zeaxanthin population transfer from S* to S_1 ($2^1A_g^-$) was required to obtain a reasonable fit to the transient spectral datasets. The same process was also invoked to explain room-temperature ultrafast transient absorption data on synthetic caroteno-phthalocyanine systems having carotenoid moieties with nine, ten, and eleven conjugated carbon−carbon double bonds.[58] The data on those systems revealed that the time constant for transfer from S* to S_1 ($2^1A_g^-$) did not show a specific trend (from 1.1 to 4 to 1.4 ps) as the extent of π-electron conjugation was increased. However, the

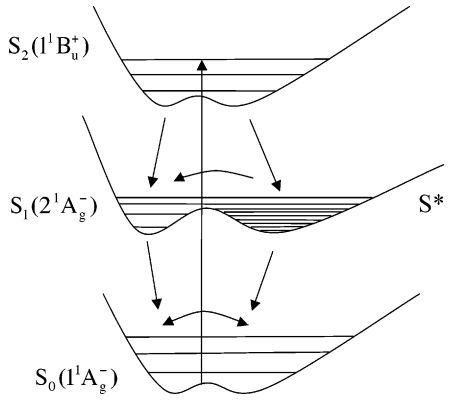

Figure 10. Simplified schematic representation of the potential energy surfaces of the xanthophylls and the branched decay to S_1 ($2^1A_g^-$) and S* from photoexcited S_2 ($1^1B_u^+$).

present data show that the S* to S_1 ($2^1A_g^-$) transfer rate at room temperature is significantly faster than at 77 K (Figure 9). Previous experimental work on these same molecules and computations on β-carotene and spirilloxanthin have proposed that S* is a twisted conformational form of S_1 ($2^1A_g^-$).[11,31] The temperature dependence of the S* to S_1 ($2^1A_g^-$) transfer rate observed here are thus suggestive of a model whereby conversion takes place on a potential energy surface possessing an activation barrier separating the S* and S_1 ($2^1A_g^-$) minima. This is illustrated in Figure 10. One question is whether conformational twisting occurs in S_2 ($1^1B_u^+$) after photoexcitation or in S_0 ($1^1A_g^-$) prior to photoexcitation. The results of the global fitting reveal similar S_2 ($1^1B_u^+$) → S_1 ($2^1A_g^-$) and S_2 ($1^1B_u^+$) → S* rate constants, k_2 and k_2' at both room temperature and 77 K, suggesting that subpopulations of twisted conformers already exist in the ground state. A similar model invoking an inhomogeneous ground state population was shown by previous

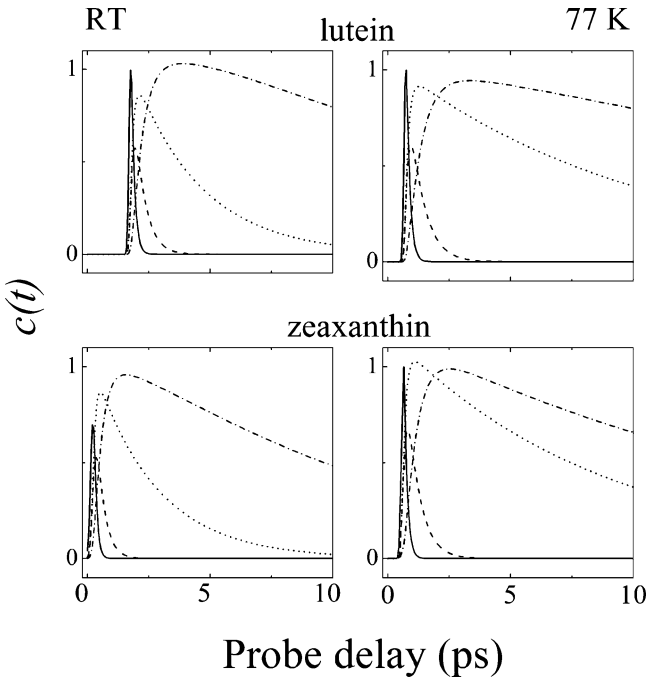

Figure 11. Time-dependent profiles of the relative concentrations, $c(t)$, of the excited states, S_2 (solid line), vibrationally excited S_1 ($2^1A_g^-$) (dashed line), S* (dotted line), and relaxed S_1 ($2^1A_g^-$) (dash-dotted line).

work to be consistent with both time-resolved and intensity-dependent data from the carotenoid, rhodopin glucoside, in the LH2 complex from *Rhodopseudomonas acidophila*.[33] Upon excitation into the S_2 ($1^1B_u^+$) state, the different conformers populate their respective S_1 ($2^1A_g^-$) and S* states and then ultimately relax back to the ground state. Here, some portion of the twisted (S*) population undergoes a conformational change along the S*-S_1 ($2^1A_g^-$) potential energy surface converting the xanthophylls into the S_1 ($2^1A_g^-$) state conformation prior to decaying back to the ground state.

As previously mentioned, the broad spectral feature that appears as a shoulder on the short-wavelength side of the main transient absorption band in the spectra taken at room temperature[31] and revealed in the third SADS of target model 2 (dark solid lines in Figure 8) sharpens considerably and shifts substantially to longer wavelength at 77 K. This feature is associated with an excited-state transition originating from the S* state, and its amplitude depends on temperature (Figure 8). This is seen more clearly in Figure 11, which displays the time-dependent concentration profiles of the different excited states obtained from target model 2. The dotted lines in the figure represent the profiles for the buildup and decay of the S* state population, and the dashed-dotted lines represent the same profiles for the S_1 ($2^1A_g^-$) state. The ratio of the maxima in the S* profile to that in the S_1 ($2^1A_g^-$) profile for each molecule can be taken as a measure of the relative yield of S*. The average ratio at 77 K is 1.00 ± 0.04 and significantly higher than the value of 0.86 ± 0.04 at room temperature. This shows that the relative yield of S* compared to S_1 ($2^1A_g^-$) increases as the temperature is lowered. Because the global fits reveal the k_2 and k_2' values associated with decay from S_2 ($1^1B_u^+$) to be comparable, this observation is not due to changes in the branching ratio from S_2 to S_1 ($2^1A_g^-$) and S* but instead is due to a decrease in the k_{31} rate constant for conversion of S* into S_1 ($2^1A_g^-$) as the temperature is lowered. This is consistent not only with the notion that S* to S_1 ($2^1A_g^-$) transfer does indeed occur, as has been suggested by other workers,[58] but that it is an activated process as illustrated in Figure 10.

Acknowledgment. This work is supported in the laboratory of HAF by the National Science Foundation (MCB-0314380). Partial support for components of the ultrafast laser spectrometer system was also provided by a grant to HAF from the National Institutes of Health (GM-30353).

Supporting Information Available: Details of target analysis modeling. This material is available free of charge via the Internet at http://pubs.acs.org.

References and Notes

(1) Isler, O. *Carotenoids*; Birkhauser: Basel, Switzerland, 1971.
(2) Frank, H. A.; Young, A. J.; Britton, G.; Cogdell, R. J. The Photochemistry of Carotenoids. In *Advances in Photosynthesis*; Govindjee, Ed.; Kluwer Academic Publishers: Dordrecht, The Netherlands, 1999; Vol. 8.
(3) Krinsky, N. I. Function. In *Carotenoids*; Isler, O., Guttman, G., Solms, U., Eds.; Birkhauser Verlag: Basel, Switzerland, 1971; pp 669.
(4) Demmig-Adams, B.; Adams, W. W., III. The xanthophyll cycle. In *Carotenoids in Photosynthesis*; Young, A. J., Britton, G., Eds.; Chapman and Hall: London, 1993; pp 206.
(5) Niyogi, K. K.; Björkman, O.; Grossman, A. R. *Proc. Natl. Acad. Sci. U.S.A.* **1997**, *94*, 14162.
(6) Gradinaru, C. C.; Kennis, J. T. M.; Papagiannakis, E.; van Stokkum, I. H. M.; Cogdell, R. J.; Fleming, G. R.; Niederman, R. A.; van Grondelle, R. *Proc. Natl. Acad. Sci. U.S.A.* **2001**, *98*, 2364.
(7) Papagiannakis, E.; Kennis, J. T. M.; van Stokkum, I. H. M.; Cogdell, R. J.; van Grondelle, R. *Proc. Nat. Acad. Sci. U.S.A.* **2002**, *99*, 6017.
(8) Papagiannakis, E.; Das, S. K.; Gall, A.; Stokkum, I. H. M.; Robert, B.; van Grondelle, R.; Frank, H. A.; Kennis, J. T. M. *J. Phys. Chem. B* **2003**, *107*, 5642.
(9) Larsen, D. S.; Papagiannakis, E.; van Stokkum, I. H. M.; Vengris, M.; Kennis, J. T. M.; van Grondelle, R. *Chem. Phys. Lett.* **2003**, *381*, 733.
(10) Polívka, T.; Sundström, V. *Chem. Rev.* **2004**, *104*, 2021.
(11) Niedzwiedzki, D. M.; Sullivan, J. O.; Polivka, T.; Birge, R. R.; Frank, H. A. *J. Phys. Chem. B* **2006**, *110*, 22872.
(12) Hudson, B.; Kohler, B. *Ann. Rev. Phys. Chem.* **1974**, *25*, 437.
(13) Hudson, B. S.; Kohler, B. E.; Schulten, K. Linear polyene electronic structure and potential surfaces. In *Excited States*; Lim, E. D., Ed.; Academic Press: New York, 1982; Vol. 6; pp 1.
(14) Frank, H. A.; Cogdell, R. J. The photochemistry and function of carotenoids in photosynthesis. In *Carotenoids in Photosynthesis*; Young, A., Britton, G., Eds.; Springer-Verlag: London, 1993; pp 252.
(15) Christensen, R. L.; Barney, E. A.; Broene, R. D.; Galinato, M. G. I.; Frank, H. A. *Arch. Biochem. Biophys.* **2004**, *430*, 30.
(16) Pariser, R. *J. Chem. Phys.* **1955**, *24*, 250.
(17) Callis, P. R.; Scott, T. W.; Albrecht, A. C. *J. Chem. Phys.* **1983**, *78*, 16.
(18) Birge, R. R. *Accts. Chem. Res.* **1986**, *19*, 138.
(19) Schulten, K.; Karplus, M. *Chem. Phys. Lett.* **1972**, *14*, 305.
(20) Tavan, P.; Schulten, K. *J. Chem. Phys.* **1979**, *70*, 5407.
(21) Andersson, P. O.; Gillbro, T. *J. Chem. Phys.* **1995**, *103*, 2509.
(22) Sashima, T.; Nagae, H.; Kuki, M.; Koyama, Y. *Chem. Phys. Lett.* **1999**, *299*, 187.
(23) Sashima, T.; Koyama, Y.; Yamada, T.; Hashimoto, H. *J. Phys. Chem. B* **2000**, *104*, 5011.
(24) Zhang, J.-P.; Inaba, T.; Watanabe, Y.; Koyama, Y. *Chem. Phys. Lett.* **2000**, *332*, 351.
(25) Fujii, R.; Ishikawa, T.; Koyama, Y.; Taguchi, M.; Isobe, Y.; Nagae, H.; Watanabe, Y. *J. Phys. Chem. A* **2001**, *105*, 5348.
(26) Furuichi, K.; Sashima, T.; Koyama, Y. *Chem. Phys. Lett.* **2002**, *356*, 547.
(27) Cerullo, G.; Polli, D.; Lanzani, G.; De Silvestri, S.; Hashimoto, H.; Cogdell, R. J. *Science* **2002**, *298*, 2395.
(28) Fujii, R.; Inaba, T.; Watanabe, Y.; Koyama, Y.; Zhang, J. P. *Chem. Phys. Lett.* **2003**, *369*, 165.
(29) Wohlleben, W.; Buckup, T.; Herek, J. L.; Cogdell, R. J.; Motzkus, M. *Biophys. J.* **2003**, *85*, 442.
(30) Wohlleben, W.; Buckup, T.; Hashimoto, H.; Cogdell, R. J.; Herek, J. L.; Motzkus, M. *J. Phys. Chem. B* **2004**, *108*, 3320.
(31) Niedzwiedzki, D.; Koscielecki, J. F.; Cong, H.; Sullivan, J. O.; Gibson, G. N.; Birge, R. R.; Frank, H. A. *J. Phys. Chem. B* **2007**, *111*, 5984.
(32) Polívka, T.; Pullerits, T.; Frank, H. A.; Cogdell, R. J.; Sundström, V. *J. Phys. Chem. B* **2004**, *108*, 15398.
(33) Papagiannakis, E.; van Stokkum, I. H.; Vengris, M.; Cogdell, R. J.; van Grondelle, R.; Larsen, D. S. *J. Phys. Chem. B* **2006**, *110*, 5727.
(34) Billsten, H. H.; Pan, J.; Sinha, S.; Pascher, T.; Sundström, V.; Polívka, T. *J. Phys. Chem. A* **2005**, *109*, 6852.

(35) de Weerd, F. L.; van Stokkum, I. H. M.; van Grondelle, R. *Chem. Phys. Lett.* **2002**, *354*, 38.
(36) Billsten, H. H.; Zigmantas, D.; Sundström, V.; Polívka, T. *Chem. Phys. Lett.* **2002**, *355*, 465.
(37) Pendon, Z. D.; Gibson, G. N.; van der Hoef, I.; Lugtenburg, J.; Frank, H. A. *J. Phys. Chem. B* **2005**, *109*, 21172.
(38) Ilagan, R. P.; Christensen, R. L.; Chapp, T. W.; Gibson, G. N.; Pascher, T.; Polivka, T.; Frank, H. A. *J. Phys. Chem. A* **2005**, *109*, 3120.
(39) van Stokkum, I. H. M.; Larsen, D. S.; van Grondelle, R. *Biochim. Biophys. Acta* **2004**, *1657*, 82.
(40) Frank, H. A.; Cua, A.; Chynwat, V.; Young, A.; Gosztola, D.; Wasielewski, M. R. *Photosynth. Res.* **1994**, *41*, 389.
(41) Polívka, T.; Herek, J. L.; Zigmantas, D.; Akerlund, H. E.; Sundström, V. *Proc. Nat. Acad. Sci. U.S.A.* **1999**, *96*, 4914.
(42) Billsten, H. H.; Bhosale, P.; Yemelyanov, A.; Bernstein, P. S.; Polivka, T. *Photochem. Photobiol.* **2003**, *78*, 138.
(43) Billsten, H. H.; Sundström, V.; Polívka, T. *J. Phys. Chem. A* **2005**, *109*, 1521.
(44) Papagiannakis, E.; van Stokkum, I. H. M.; van Grondelle, R. *J. Phys. Chem. B* **2003**, *107*, 11216.
(45) Tavan, P.; Schulten, K. *J. Chem. Phys.* **1986**, *85*, 6602.
(46) Koyama, Y.; Kuki, M.; Andersson, P. O.; Gillbro, T. *Photochem. Photobiol.* **1996**, *63*, 243.
(47) Christensen, R. L.; Kohler, B. E. *Photochem. Photobiol.* **1973**, *18*, 293.
(48) Kohler, B. E. Electronic structure of Carotenoids. In *Carotenoids*; Britton, G., Liaaen-Jensen, S., Pfander, H., Eds.; Birkhäuser Verlag AG: Basel, Switzerland, 1995; Vol. 1B: Spectroscopy; pp 3.
(49) Meyer, B. *Low temperature spectroscopy*; American Elsevier: New York, 1971.
(50) Turro, N. J. *Modern Molecular Photochemistry*; University Science Books: CA, 1991.
(51) Josue, J. S.; Frank, H. A. *J. Phys. Chem. A* **2002**, *106*, 4815.
(52) Hashimoto, H.; Koyama, Y. *Chem. Phys. Lett.* **1989**, *154*, 321.
(53) Hashimoto, H.; Koyama, Y.; Hirata, Y.; Mataga, N. *J. Phys. Chem.* **1991**, *95*, 3072.
(54) Simpson, J. H.; McLaughlin, L.; Smith, D. S.; Christensen, R. L. *J. Chem. Phys.* **1987**, *87*, 3360.
(55) Kohler, B. E.; Spangler, C.; Westerfield, C. *J. Chem. Phys.* **1988**, *89*, 5422.
(56) Englman, R.; Jortner, J. *Mol. Phys.* **1970**, *18*, 145.
(57) Chynwat, V.; Frank, H. A. *Chem. Phys.* **1995**, *194*, 237.
(58) Berera, R.; van Stokkum, I. H.; Kodis, G.; Keirstead, A. E.; Pillai, S.; Herrero, C.; Palacios, R. E.; Vengris, M.; van Grondelle, R.; Gust, D.; Moore, T. A.; Moore, A. L.; Kennis, J. T. *J. Phys. Chem. B* **2007**, *111*, 6868.